Available online at www.sciencedirect.com

ScienceDirect

Proceedings of the Combustion Institute 37 (2019) 5113–5120

Proceedings of the Combustion Institute

www.elsevier.com/locate/proci

Flame dynamics of azimuthal forced spinning and standing modes in an annular combustor

Håkon T. Nygård*, Marek Mazur, James R. Dawson, Nicholas A. Worth

Department of Energy and Process Engineering, Norwegian University of Science and Technology, Trondheim N-7491, Norway

Received 30 November 2017; accepted 20 August 2018
Available online 8 September 2018

Abstract

Azimuthal forcing has been applied to flames in a laboratory scale annular combustor in order to accurately control the azimuthal mode of excitation. A new forcing configuration permitted not only the pressure amplitude, but also the spin ratio and mode orientation to be accurately controlled, in order to generate standing modes and for the first time strong spinning modes in both a clockwise (CW) and anti-clockwise (ACW) direction. The phase averaged heat release dynamics of these modes was compared and a number of differences observed depending on the direction of pressure wave propagation, demonstrating characteristic ACW and CW heat release patterns. A new spin compensating averaging method was then introduced to analyse the flame dynamics, and it was shown that through the application of this method the dynamics of standing wave oscillations could be decomposed to recover the characteristic ACW and CW heat release responses. The global heat release response was also assessed during strongly spinning modes, and the magnitude of the response was shown to depend strongly on the direction of propagation, demonstrating the importance of the local swirl direction on the global heat release response, with important implications for the modelling of such flows.

Keywords: Gas turbines; Azimuthal modes; Combustion instabilities; Acoustic forcing; Flame dynamics

1. Introduction

The issue of thermoacoustic instability can arise during the development of new gas turbine engines, or when operating existing engines in new regimes, for example in order to reduce emissions or increase fuel flexibility. Damaging levels of pressure and heat release oscillations can occur during these instabilities, and therefore there is a need to eliminate these at the design stage, motivating the need for a greater understanding of the phenomenon.

A number of recent studies have focused on the advent of such instabilities in annular geometry [1–4], where the excitation of azimuthal modes results in flame responses which are no longer solely controlled by the magnitude and frequency of pressure oscillations, but also by characteristics

* Corresponding author.
E-mail address: hakon.t.nygard@ntnu.no (H.T. Nygård).

https://doi.org/10.1016/j.proci.2018.08.034

of the acoustic mode, such as the standing wave ratio (commonly referred to as the spin ratio [2]) and the orientation of the mode relative to flames. Previous studies in annular geometry have recently identified well defined modal preferences for different oscillation types, where changes to the chamber geometry, equivalence ratio and bulk flow velocities can result in significant changes to the modal dynamics observed [5–9]. To further complicate matters, recent studies have also shown that these modal characteristics may vary with time, leading to rapid switching between predominantly spinning and standing states [3,5,10,11] and rapid changes in orientation [8]. It has been shown in recent studies [12–14] that a small breaking in symmetry can greatly influence which mode is dominating. For example, in [12] non-uniformities in the heat release and pressure coupling resulted in a preference for spinning modes for weak non-uniformities and standing modes for sufficiently large non-uniformities. Furthermore, in [13] it was found the standing mode is related to either combustors that are non-rotationally symmetric, weak flame response at low amplitudes and strong response at large amplitudes or other physical mechanisms such as a mean azimuthal flow affecting the flame response. Symmetry breaking was found to promote standing modes in [14], while the addition of a mean azimuthal flow promote spinning modes.

Azimuthal pressure waves can induce local transverse velocity oscillations which can affect the flame dynamics and the spatial distribution of the heat release rate [15,16]. Therefore, in order to fully quantify the heat release response of an annular combustor there is a need to understand and ultimately predict the dynamic response of each flame to different modes of excitation. A greater knowledge of the flame response to different modes of oscillation may help us to construct models of the heat release response, which when integrated in low order network models [17–19] or as part of more involved Helmholtz calculations [20] represent both a viable and promising method of predicting system stability. Such flame describing functions (FDF) have previously been calculated experimentally [2,11], or numerically through either high fidelity simulations [21] or flame front modelling [22,23]. However, the prediction of such functions, particularly with lower order approaches, is still far from resolved, and a greater understanding of the flame dynamics should be considered invaluable to the further development of these methods. Furthermore, a better phenomenological understanding may also help us to understand how and why mode switching occurs in annular chambers, and help us to draw links between underlying flow behaviour and the modal dynamics in such systems.

Rapid mode switching in annular chambers makes isolating and studying the flame dynamics in annular configurations very challenging. Studies of self-excited instabilities are forced to rely on conditional averaging which reduces the amount of available data at each condition, but more crucially may only cover a small subset of the possible range of azimuthal mode characteristics. One way to address this issue is to prescribe the mode of excitation through the application of acoustic forcing. Recently transverse acoustic forcing has been applied in order to investigate the flame response to the orientation of pressure disturbances [24–26]. More recently, acoustic forcing of azimuthal modes in annular chambers have been undertaken, first in an annular chamber fitted with electrically heated Rijke tubes [27] and then later in annular combustor [28].

The present paper seeks to further our understanding of the flame dynamics in annular chambers through the application of azimuthal forcing to a laboratory scale annular combustor. When operated in a self-excited state, the current combustor exhibits a strong preference for anticlockwise (ACW) spinning modes [5], making the study of self-excited spinning modes in the clockwise (CW) direction almost impossible. Azimuthal forcing has been used to generate and analyse for the first time strong spinning modes in both directions for a reacting flow setup and relate the structure and dynamics of these oscillations to standing wave oscillations. Studying the heat release distribution and flame dynamics for a prescribed mode of excitation will eventually help predicting the growth rate and amplitude of the limit cycle of the instabilities. The ability to study modes of excitation which do not naturally occur allow important observations on the dynamics of spinning modes to be made, and for the first time give us the ability to accurately quantify these.

2. Experimental methods

2.1. Annular combustor and data acquisition

The annular combustor used in this study is described in detail in [1]. In the current study it is operated with a premixed air-ethylene mixture at an equivalence ratio of $\phi = 0.75$ and a bulk exit velocity of approximately 20ms^{-1} at the injector exit. Operation at this equivalence ratio ensures the flow is not self-excited, resulting in better modal control. In the current configuration, as shown in Fig. 1, the combustor consists of a cylindrical plenum chamber ($D_\text{p} = 212\text{mm}$, $L_\text{p} = 200\text{mm}$) with honeycomb flow straightener and grids to condition the flow. A hemispherical body ($D_\text{h} = 140\text{mm}$) aids flow distribution to each burner. 18 injectors ($d_\text{exit} = 18\text{mm}$) are equally spaced around a circle of diameter $d_\text{c} = 170\text{mm}$, and each features a centrally located bluff body ($d_\text{bb} = 13\text{mm}$). Each bluff

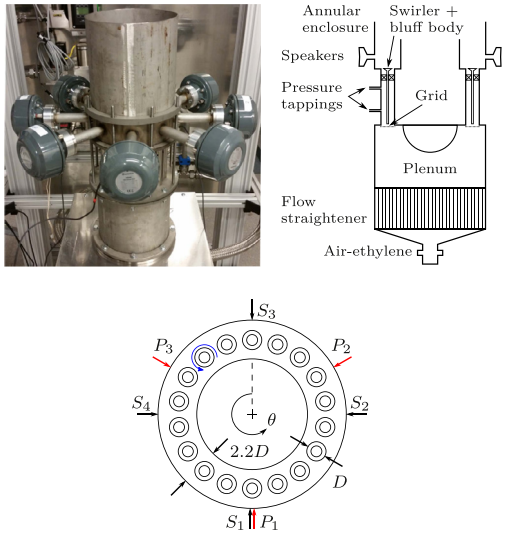

Fig. 1. Annular combustor with forcing array. *left top* combustor image (every other speaker used for forcing); *right top* schematic side view; *bottom* schematic top view. S_i and P_k mark the angular positions of speakers and transducers. S_1 and P_1 are located at $\theta = 180^\circ$, with 90° between each speaker used and 120° between each transducer. Direction of swirl is indicated by the blue arrow. (For interpretation of the references to colour in this figure legend, the reader is referred to the web version of this article.)

body features a six vane, $\alpha = 60^\circ$ anti-clockwise swirler mounted 10mm upstream measured from the dump plane to the swirler trailing edge. The annular chamber consists of inner and outer cylinders of diameter $D_\mathrm{i} = 129$mm and $D_\mathrm{o} = 212$mm, which extend 130mm and 300mm downstream of the dump plane respectively.

Three Kulite XCS-093-05D pressure transducers are mounted flush with the inner wall of the injector tubes 45mm below the dump plane at the angular locations marked by P_k in Fig. 1. The transducer signals are amplified by a Fylde FE-579-TA bridge amplifier, before being logged using NI-9234 24-bit DAQ cards with sampling frequency $f_\mathrm{trans} = 51.2$kHz. The heat release fluctuations are recorded through OH* chemiluminescence using a Photron SA1.1 CMOS camera with a LaVision Intensified Relay Optics unit and a Cerco 2178 UV lens equipped with a D20-VG0035942 filter (centre wavelength 310nm, full width half maximum 10nm). The camera was operated with sampling frequency $f_\mathrm{cam} = 10$kHz at a 768×768 pixels resolution (resulting in a spatial resolution of 3.2 pixels/mm) and a total of 19, 410 images were recorded.

2.2. Mode determination

Assuming the acoustic mode in the combustor is a superposition of two counter rotating 1D plane waves with wavelength corresponding to the unwrapped length of the combustor, the complex pressure fluctuations can be expressed as $p(\theta_k, t) = \left[A_+ e^{\mathrm{i}(\theta_k - v_\theta t/R)} + A_- e^{\mathrm{i}(-\theta_k + v_\theta t/R)}\right] e^{\mathrm{i}\omega_0 t}$. A_+ and A_- are the amplitudes of the ACW and CW rotating waves respectively, where θ_k is the angle of the kth sensor, as defined in Fig. 1, ω_0 is the forcing angular frequency and v_θ/R is the angular velocity of the nodal line if there is a standing wave component. The pressure fluctuation amplitude of any given mode is given by $\left[A_+^2 + A_-^2\right]^{1/2}$. The pressure measured from each pressure transducer is the real part of the complex pressure, $p_\mathrm{meas} = \mathrm{Re}\{p\}$. To determine all the unknowns in the equation, a nonlinear least squares fit is applied to the indicator $C(t) = \frac{1}{N}\sum_{k=1}^{N} \mathrm{Re}\left\{p(\theta_k, t) e^{\mathrm{i}\theta_k}\right\}$, which was introduced in [10]. To differentiate between predominantly spinning and standing modes, the spin ratio $SR = (|A_+| - |A_-|)/(|A_+| + |A_-|)$ is used [2], with the following scheme applied to classify modes which are predominantly spinning in either the CW ($SR < -1/3$) or ACW ($SR > 1/3$) directions, or otherwise standing. The value of $\pm 1/3$ corresponds to the largest pressure amplitude of the two travelling waves being twice the lowest and is chosen to be consistent with previous work [29].

2.3. Forcing setup

The forcing array, shown in Fig. 1, consists of eight 120mm long standoff tubes, mounted at a height of 35mm above the dump plane and spaced equidistantly around the chamber. Each standoff tube has a horn driver (Adastra HD60 16Ω) mounted at the end, with diametrically opposite drivers forced in anti-phase forming a speaker pair. A multi channel waveform generator Aim-TTI TGA1244 was used to create synchronised forcing outputs which were amplified using QTX PRO 1000 amplifiers. In the present investigation the two speaker pairs indicated in Fig. 1, and thus only every other horn driver, are used to set up the acoustic modes, simplifying the setup process while still giving good control. Given ideal geometry and speaker response, if all forcing amplitudes were equal, zero phase delay would be used to produce standing modes, while a phase delay of $\pm 90\circ$ would be used to produce spinning modes. In practice the amplitude and phase delay between the speakers were adjusted carefully to achieve the desired amplitude response, and mode type and orientation.

2.4. Spin compensating rotational averaging

Forcing different azimuthal modes in the presence of a turbulent reacting flow has been shown

to lead to stochastic fluctuations in the pressure response and spin ratio [28] when compared to cold flow conditions. Therefore, in order to investigate the phase averaged component of the heat release that is moving at a constant rate in a given direction, a new rotational averaging method is introduced in the current paper.

As in previous work, initially the phase averaged normalised heat release fluctuation $\tilde{Q}_n = ((\tilde{Q} - \overline{Q})/\langle \overline{Q} \rangle)$ is calculated based on the pressure signals. Here $\tilde{Q}_n = \tilde{Q}_n(r, \theta, \tau/T)$, where τ/T is the normalised position in the phase averaged cycle, $Q = Q(r, \theta, t)$ is the spatial distribution of OH^* intensity captured by the camera, and $\tilde{Q} = \tilde{Q}(r, \theta, \tau/T)$ is its phase average, $\overline{Q} = \overline{Q}(r, \theta)$ is the temporal mean and $\langle \overline{Q} \rangle$ is the spatial and temporal mean. Phase averaging is highly applicable given the typical self-excited response in the current combustor is dominated by oscillations at a single frequency [5], as are the forced oscillations.

For a general case using N burners one forcing cycle is divided into a total of N time steps for phase averaging. In order to isolate the spinning component in a given direction the jth phase average distribution is rotated by an angle $2\pi j/N$ in the opposite direction to the prescribed direction of interest. Since N time steps are used the burners will overlap after the rotation, and the transformation effectively freezes the propagation of any spinning component in the prescribed direction. This is done under the assumption of heat release patterns moving at the same constant speed in both directions. The assumption can be made due to the induced bulk swirl being at least two orders of magnitude lower than the speed of sound, making a negligible difference in propagation speed for the two plane waves. The average of the N rotated distributions is then calculated according to Eq. (1), producing a single spatial spin compensated distribution, $\overline{Q}^{\mathrm{x}}_{\mathrm{rot}} = f(r, \theta)$.

$$\overline{Q}^{\mathrm{x}}_{\mathrm{rot}} = \frac{1}{N} \sum_{j=0}^{N-1} \mathrm{Rot}_{\beta_j} \left\{ \left[\frac{\tilde{Q} - \overline{Q}}{\langle \overline{Q} \rangle} \right]_j \right\}, \tag{1}$$

where x is either the ACW or the CW component, j is the phase average time step and Rot_{β_j} is a rotation of β_j around the center of the annulus. The angle is calculated as $\beta_j = \pm \frac{2\pi}{N} j$, where positive and negative signs are used for CW and ACW components respectively.

The summation of these rotated images effectively averages the heat release distribution of each of the N flames at the same point in the cycle, in the direction of rotation. Oscillations travelling in the opposite direction are effectively cancelled, making the method invaluable for isolating and studying the effect of spinning waves travelling in different directions around the annulus. The method also offers an advantage in that slight variations in heat release from flame to flame are also averaged out, providing a clearer description of the mean flame response to acoustic waves and retaining finer structural details of the heat release rate.

In the rest of the paper $\overline{Q}^{\mathrm{ACW}}_{\mathrm{rot}}$ and $\overline{Q}^{\mathrm{CW}}_{\mathrm{rot}}$ will be used to describe the spin compensated averages of the normalised phase average heat release oscillations in the ACW and CW directions respectively.

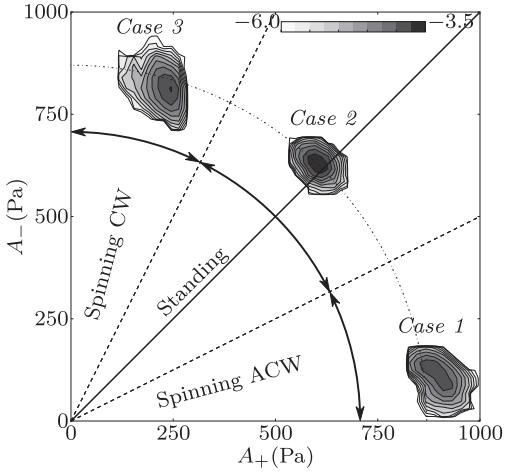

Fig. 2. Joint PDF of A_+ and A_- for three different cases, all using forcing frequency $f_0 = 1690$Hz. Dashed lines indicate $SR = \pm 1/3$ and the solid line is $SR = 0$. Case 1: $\overline{SR} = 0.9$; Case 2: $\overline{SR} = 0.0$; Case 3: $\overline{SR} = -0.6$. Intensity contours describe base 10 exponentials.

3. Results and discussion

3.1. Acoustically forced modes

Azimuthal acoustic forcing was applied in order to investigate the flame dynamics of the following three different oscillation modes: *Case 1.* Strongly spinning in the ACW direction; *Case 2.* Predominantly Standing; *Case 3.* Strongly spinning in the CW direction. In order to assess the pressure response of these forced cases Fig. 2 shows the joint probability density function (JPDF) of the two counter rotating waves A_+ and A_-. The centre of the JPDF distributions for the three cases shows that the application of acoustic forcing is sufficient to exercise good control over the mode of oscillation, and generate as desired distinct standing and spinning modal responses. Although a high level of sensitivity to forcing parameters resulted in a larger spin ratio in the ACW direction in comparison with the CW direction, it should be noted that both cases can be considered strongly spinning, with a ratio between ACW and CW travelling waves of over 4 times. All cases have approximately the same mean pressure fluctuation amplitude, meaning the acous-

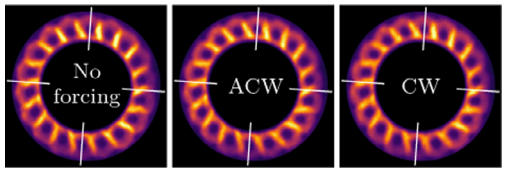

Fig. 3. Mean flame structure for the no forcing case (left), and the ACW spinning (middle) and the CW spinnning (right) forced modes. The white lines represent the location of the speakers used for forcing.

tic energy fed into the system is of similar magnitude for all cases. This amplitude was selected to be similar to previously observed self-excited modes observed in the combustor [5]. Finally it should be noted that while the size of the probability distributions for all cases is significantly smaller than those observed during the study of self-excited instabilities, the finite size of these still indicates the presence of some unsteady mode switching, which is consistent with previous work [28].

3.2. Mean flame structure

The mean OH* chemiluminescence of unforced and spinning mode cases is shown in Fig. 3. As seen in previous investigations, the regions of highest heat release are observed between adjacent flames. While the heat release distribution is strongly asymmetric around each flame, there is rotational symmetry from flame to flame. Comparison between unforced and spinning mode cases shows no significant qualitative differences in the distributions, suggesting the forcing does not significantly affect the mean flame structure, which is consistent with previous investigations [28].

3.3. Flame dynamics of azimuthally forced modes

The flame dynamics of the acoustically forced modes have been studied through snapshots of the phase average heat release distribution and through the application of the new spin compensating average procedure described in §2.4. Figure 4 shows snapshots of the phase average heat release oscillations at a single location in the pressure cycle in the left column for all three forced cases. In the two middle columns the spin compensated distributions in both directions for the same cases are shown with zoomed in versions of selected cases in the rightmost column.

Observing the snapshot for the strong ACW mode, *Case 1* in the left column of Fig. 4, the heat release oscillations are qualitatively similar to those observed during self-excited instabilities [1]. The largest fluctuations are appearing close to the outer radial wall in a large band-like structure which spans almost half the annulus, and large oscillations are also produced in the interacting region between adjacent flames. Such structures have been linked previously to the formation of coherent vortical structures in the shear layers as a response to the pressure oscillations in the chamber [15]. The close agreement with previous results suggests the acoustic forcing of spinning waves produces a similar flame response to self-excited fluctuations.

While the use of acoustic forcing allows good control over the spin ratio, increasing the amount of data used for phase averaging and therefore the clarity of the imaging, the use of spin compensating averaging further improves clarity, and also allows the decomposition of oscillations to be investigated. Comparing the two centre images for the upper and lower rows in Fig. 4, the averaged component traveling in the direction of forcing is shown to dominate over the component in the counter direction (Strong oscillations are therefore observed in $\overline{Q}^{\mathrm{ACW}}_{\mathrm{rot}}$ and $\overline{Q}^{\mathrm{CW}}_{\mathrm{rot}}$ for the ACW and CW spinning cases respectively). The residual oscillations observed in the counter direction averages may arise due to the imperfect spinning waves generated in the present study (as seen in Fig. 2) or non uniformity between burners. The heat release structure of both ACW and CW components is similar to the phase averaged snapshots, but the averaging procedure removes burner to burner differences, making observations of the structure much clearer, highlighting the difference between the cases. Allowing the entire phase average cycle to be collapsed onto one image also allows a more straightforward comparison of the magnitude of the response, and a slight decrease in oscillation amplitude of the most intense structure is observed for the CW spinning case.

It is interesting to contrast the response in *Case 1* featuring a strong ACW mode with that of *Case 3* which features a strong CW spinning wave. The CW case occurs rarely when the combustor is self-excited [5], and therefore the use of acoustic forcing presents the only viable method of studying the flame response. Comparing the zoomed in views in Fig. 4 of the two spinning modes the main features are quite similar, but with a number of subtle differences. The flame response to the CW spinning wave is again very asymmetric, with the largest heat release oscillations observed close to the outer wall and between adjacent flames. However, the structures appear to be more isolated in comparison with the linked structure produced by the ACW spinning wave, with breaks visible between adjacent flames. Furthermore, the largest heat release oscillations are observed to move from the outer radial wall to the interacting region between adjacent flames and more activity is also observed close to the inner wall, representing a spatial shift in the centre of heat release in the radial direction. Another difference that can be observed is the presence of linked structure between the bluff body and the interacting region for the CW case that is much weaker for the ACW case (black squares in zoomed

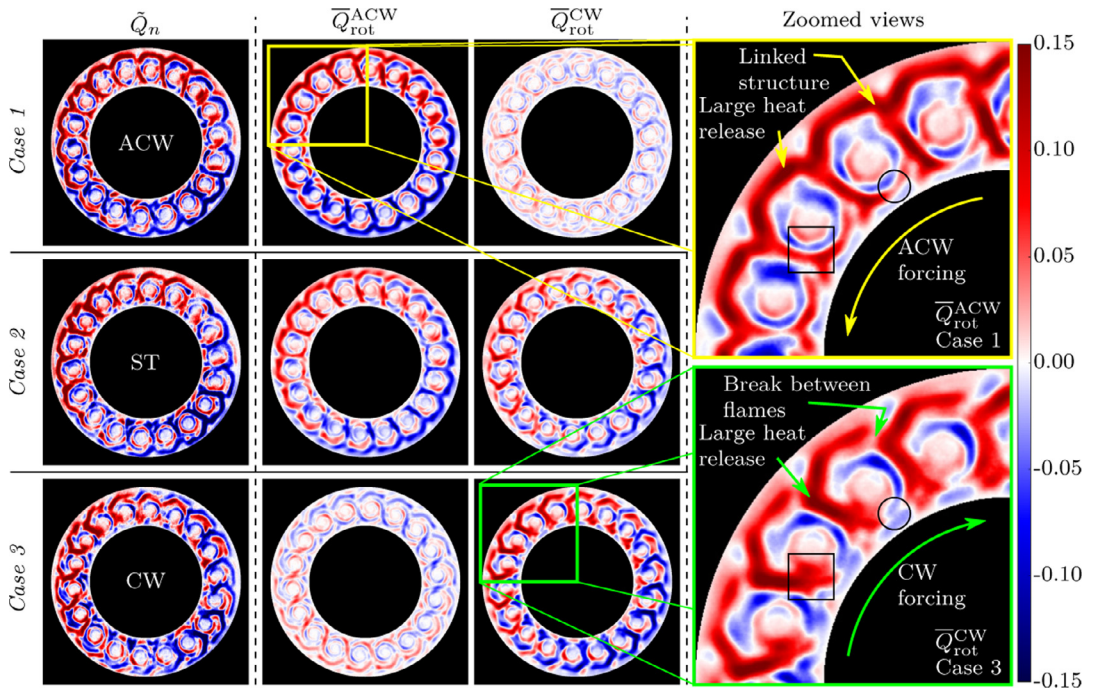

Fig. 4. Snapshot of phase average in left column, with the spin compensating average in both directions in the two middle columns. Each row represents one forcing case and for ease of comparison the regions of maximum heat release have been aligned. Top: Strong ACW forcing (*Case 1*); middle: Standing mode (*Case 2*); bottom: Strong CW forcing (*Case 3*). The right column is annoted and highlighted zoomed in views of two of the most interesting cases of the spin compensated average. The colour bar is valid for the whole figure. (Colour online).

views in Fig. 4). In the CW case heat release rate along the inner part of the wall is also in phase and connected with the heat release around the bluff body closest to the inner annular wall, while for the ACW case there is a clear division between them (black circles in zoomed views in Fig. 4). The major difference between the two spinning cases is the direction of forcing in relation to the direction of swirl. For the ACW case the acoustic forcing is in the flow direction induced by the swirlers along the outer wall, while for the CW case the forcing is in the opposite direction. The direction of the acoustic wave relative to the local swirl direction is observed therefore to have a significant effect on the flame dynamics when flames are closely confined in annular geometry.

The same spin compensating averaging procedure was also applied to the standing wave in *Case 2*, shown in the middle row (two centre images) in Fig. 4. In this case the heat release oscillations in both $\overline{Q}^{\mathrm{ACW}}_{\mathrm{rot}}$ and $\overline{Q}^{\mathrm{CW}}_{\mathrm{rot}}$ have similar magnitudes, and observation of the spatial distributions shows strong similarities with the corresponding spinning waves in *Case 1* and *Case 3* respectively. The oscillation magnitudes of these components are lower in comparison with the spinning cases, as the vector sum of pressure fluctuation amplitudes was kept constant between cases. The observation of the ability to decompose the heat release distribution during a standing wave oscillation into its constituent spinning wave components may be invaluable in further understanding the dynamics of such systems in cases where the full range of responses cannot be measured directly, and in the modelling of such responses.

3.4. Integrated heat release response

It is also useful to examine the global heat release response of each flame which is a parameter widely used in low order models. A 20° wide kernel positioned at each burner centre is used to evaluate the mean heat release over an oscillation cycle. The integration is performed on the spin compensated averages in the direction of forcing in order to evaluate the average burner behaviour for this dominant component. The sector kernel is also further divided into inner and outer regions in order to understand the local distribution of heat release between cases. The results for the two forced spinning modes are shown in Fig. 5 together with sinusoidal fitted curves, and for ease of comparison the phase of the cycles is normalised to the global integrated heat release.

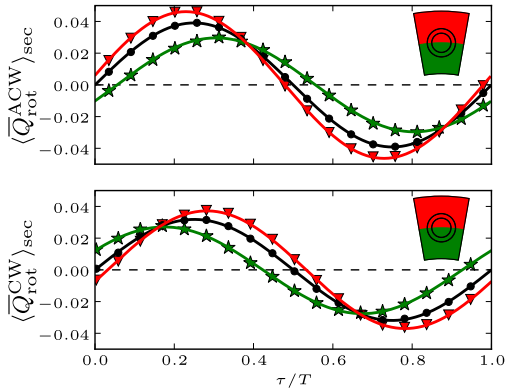

Fig. 5. Sector averaged heat release oscillations for *top* ACW and *bottom* CW spinning modes. Averages shown from inner (green line, star markers) and outer (red line, triangle marker) regions, and the total response (black line, circular markers). The markers represent measurements while the solid lines are fitted sine curves. To aid interpretation, the phase of the total heat release (black lines) for the two cases have been aligned. (For interpretation of the references to colour in this figure legend, the reader is referred to the web version of this article.)

It is interesting to examine the phase and magnitude of the inner and outer heat release oscillations. For *Case 1* for an ACW spinning mode the inner heat release oscillation is observed to lag the outer, with a phase difference of $\Delta t/T \approx 0.08$. In comparison in *Case 3* for a CW spinning mode the phase lag is inverted, and now the outer oscillation lags the inner. Significantly for this case the phase lag also increased to $\Delta t/T \approx 0.11$.

Moreover, the oscillation amplitude of the inner and outer regions are $|\langle \overline{Q}^{ACW}_{rot} \rangle_{inner}| = 0.030$ and $|\langle \overline{Q}^{ACW}_{rot} \rangle_{outer}| = 0.046$ respectively during an ACW spinning mode. In comparison for the CW spinning mode the amplitudes are $|\langle \overline{Q}^{CW}_{rot} \rangle_{inner}| = 0.027$ and $|\langle \overline{Q}^{CW}_{rot} \rangle_{outer}| = 0.037$. This quantifies the observation in the previous section that the heat release magnitude decreases and appears to shift radially inward. The amplitude ratio between outer and inner regions decreases slightly from $|\langle \overline{Q}^{ACW}_{rot} \rangle_{outer}|/|\langle \overline{Q}^{ACW}_{rot} \rangle_{inner}| = 1.6$ for the ACW case to $|\langle Q^{CW}_{rot} \rangle_{outer}|/|\langle Q^{CW}_{rot} \rangle_{inner}| = 1.4$ for the CW case, conforming broadly to spatial reorganisation of heat release observed previously [5].

The combination of increased phase lag and decreased oscillation amplitude for the CW spinning case results in an amplitude difference of around 23% for the total integrated heat release response in comparison with the ACW case. Given the slight differences in the pressure response amplitudes (shown in Fig. 2) and the spin ratios this difference may not be purely due to differences in the spinning mode orientation. To eliminate these influences a similar analysis was performed using the decomposed standing wave of case 2, ensuring the similarity of both components in terms of spin ratio and pressure response magnitude. While not included graphically for brevity, a similar difference of 35% was calculated for the total heat release response. The similarity of this adds to the qualitative evidence presented in Section 3.3 which suggests that standing waves can be decomposed into their spinning components, although further evidence will be sought in future work. Therefore, given that the main difference between cases is the orientation of swirl relative to the incoming pressure wave, the directionality of the spinning mode appears in this case to be significant. This result has important implications for low order models which use the integrated heat release response, and suggest that different flame responses may need to be defined in order to characterise CW and ACW spinning modes.

Finally it is worth observing that the sinusoidal curves fit the measurements very closely, demonstrating that sinusoidal forcing of a spinning mode results in a traveling heat release fluctuation that is also sinusoidal. While the rotational averaging assumes that the heat release rate fluctuation is azimuthally periodic, and identical burner response, it does not impose a sinusoidal response. The observed behaviour provides a further indication for how the heat release field can be linearly manipulated for the cases in the present study.

4. Conclusions

In the present study azimuthal forcing has been applied to generate for the first time well controlled spinning and standing waves in a lab scale annular combustor, allowing the flame dynamics of modes with different spin ratios to be investigated with much greater precision than previously possible. A close agreement between the dynamics of ACW spinning waves in forced and previous self-excited experiments was observed. However, a number of differences were observed between these ACW cases and the flame dynamics occurring during CW spinning waves, including the redistribution of heat release in the annulus. Observation of the integrated heat release oscillations indicated a shift from outer to inner annulus depending on direction of the spinning wave. These changes were attributed to the symmetry breaking effect of the locally swirling flow at each flame. Finally through the introduction of a novel averaging method it was shown that the heat release dynamics during a standing mode could be decomposed into ACW and CW spinning components, offering a new way of understanding the dynamics of such systems.

Acknowledgements

The authors gratefully acknowledge financial support from the European Research Council (ERC): Grant agreement 677931 TAIAC.

References

[1] N.A. Worth, J.R. Dawson, *Proc. Combust. Inst.* 34 (2) (2013) 3127–3134, doi:10.1016/j.proci.2012.05.061.

[2] J.-F. Bourgouin, D. Durox, J. Moeck, T. Schuller, S. Candel, in: Proceedings of the ASME Conference, 2013. GT2013-95010.

[3] G. Ghirardo, M.P. Juniper, *Proc. Royal Soc. A* 469 (2157) (2013), doi:10.1098/rspa.2013.0232.

[4] G. Staffelbach, L. Gicquel, G. Boudier, T. Poinsot, *Proc. Combust. Inst.* 32 (2) (2009) 2909–2916.

[5] N.A. Worth, J.R. Dawson, *Combust. Flame* 160 (11) (2013) 2476–2489, doi:10.1016/j.combustflame.2013.04.031.

[6] D. Laera, T. Schuller, K. Prieur, D. Durox, S.M. Camporeale, S. Candel, *Combust. Flame* 184 (2017) 136–152.

[7] K. Prieur, D. Durox, T. Schuller, S. Candel, *Combust. Flame* 175 (2017) 283–291.

[8] N.A. Worth, J.R. Dawson, *Proc. Combust. Inst.* 36 (3) (2017) 3743–3751.

[9] K. Prieur, D. Durox, T. Schuller, S. Candel, *J. Eng. Gas Turb. Power* 140 (3) (2018) 031503, doi:10.1115/1.4037824.

[10] P. Wolf, G. Staffelbach, L.Y. Gicquel, J.-D. Müller, T. Poinsot, *Combust. Flame* 159 (11) (2012) 3398–3413, doi:10.1016/j.combustflame.2012.06.016.

[11] N. Noiray, B. Schuermans, *Proc. Royal Soc. A* 469 (2151) (2013), doi:10.1098/rspa.2012.0535.

[12] N. Noiray, M. Bothien, B. Schuermans, *Combust. Theor. Model.* 15 (5) (2011) 585–606, doi:10.1080/13647830.2011.552636.

[13] G. Ghirardo, M.P. Juniper, J.P. Moeck, in: Proceedings of the ASME Conference, 2015. GT2015-43127.

[14] M. Bauerheim, M. Cazalens, T. Poinsot, *Proc. Combust. Inst.* 35 (3) (2015) 3219–3227, doi:10.1016/j.proci.2014.05.053.

[15] J.R. Dawson, N.A. Worth, *Combust. Flame* 161 (10) (2014) 2565–2578.

[16] V. Acharya, T. Lieuwen, *Combust. Flame* 165 (2016) 188–197, doi:10.1016/j.combustflame.2015.12.003.

[17] A.P. Dowling, *J. Fluid Mech.* 346 (1997) 271–290.

[18] S.R. Stow, A.P. Dowling, *Proceedings of the ASME Conference* (2004) 775–786. GT2004-41669.

[19] N. Noiray, D. Durox, T. Schuller, S. Candel, *J. Fluid Mech.* 615 (2008) 139–167, doi:10.1017/S0022112008003613.

[20] F. Nicoud, L. Benoit, C. Sensiau, T. Poinsot, *AIAA Journal* 45 (2) (2007) 426–441.

[21] X. Han, J. Li, A.S. Morgans, *Combust. Flame* 162 (10) (2015) 3632–3647.

[22] A. Cuquel, D. Durox, T. Schuller, in: Seventh Mediterranean Combustion Symposium, Sardinia, Italy, September, 2011, pp. 11–15.

[23] P. Palies, T. Schuller, D. Durox, S. Candel, *Proc. Combust. Inst.* 33 (2) (2011) 2967–2974.

[24] J. O'Connor, T. Lieuwen, *Combust. Sci. Technol.* 183 (2011) 427–443. 17.

[25] M. Hauser, M. Lorenz, T. Sattelmayer, *J. Eng. Gas Turb. Power* 133 (4) (2011) 041501, doi:10.1115/1.4002175.

[26] A. Saurabh, C.O. Paschereit, *Combust. Flame* 182 (2017) 298–312.

[27] G. Gelbert, J.P. Moeck, C.O. Paschereit, R. King, *Control Eng. Pract.* 20 (8) (2012) 770–782.

[28] N.A. Worth, J.R. Dawson, J.A. Sidey, E. Mastorakos, *Proc. Combust. Inst.* 36 (3) (2017) 3783–3790.

[29] J.R. Dawson, N.A. Worth, *Proc. Combust. Inst.* 35 (3) (2015) 3283–3290.